Title: Comparison of Polar Mesospheric Cloud Measurements from the Cloud Imaging and Particle Size Experiment and the Solar Backscatter Ultraviolet Instrument in 2007

Corresponding author: Susanne Benze[a]

Co-authors: Cora E. Randall[b], Matthew T. DeLand[c], Gary E. Thomas[d], David W. Rusch[e], Scott M. Bailey[f], James M. Russell, III[g], William McClintock[h], Aimee W. Merkel[i], Chris Jeppesen[j]

[a] Laboratory for Atmospheric and Space Physics & Dept of Atmospheric and Oceanic Sciences, University of Colorado at Boulder, 392 UCB, Boulder, CO 80309-0392, USA, susanne.benze@lasp.colorado.edu, phone (303)-492-3260, fax (303)-492-6946

[b] Laboratory for Atmospheric and Space Physics & Dept of Atmospheric and Oceanic Sciences, University of Colorado at Boulder, 392 UCB, Boulder, CO 80309-0392, USA, randall@lasp.colorado.edu

[c] Science Systems and Applications, Inc. (SSAI), Greenbelt, Maryland, USA, matthew_deland@ssaihq.com

[d] Laboratory for Atmospheric and Space Physics, 1234 Innovation Drive, Boulder, CO 80303, USA, gary.thomas@lasp.colorado.edu

[e] Laboratory for Atmospheric and Space Physics, 1234 Innovation Drive, Boulder, CO 80303, USA, Dave.Rusch@lasp.colorado.edu

[f] Bradley Department of Electrical and Computer Engineering, Virginia Polytechnical and State University, Blacksburg, VA 24061, USA, baileys@vt.edu

[g] Center for Atmospheric Sciences, Hampton University, Hampton, Virginia, USA, James.Russell@hamptonu.edu

[h] Laboratory for Atmospheric and Space Physics, 1234 Innovation Drive, Boulder, CO 80303, USA, William.McClintock@lasp.colorado.edu

[i] Laboratory for Atmospheric and Space Physics, 1234 Innovation Drive, Boulder, CO 80303, USA, aimee.merkel@lasp.colorado.edu

[j] Laboratory for Atmospheric and Space Physics, 1234 Innovation Drive, Boulder, CO 80303, USA, jeppesen@lasp.colorado.edu

Potential reviewers:

Jerry Lumpe (lumpe@cpi.com)

John Olivero (oliveroj@erau.edu)

Eric Shettle (shettle@nrl.navy.mil)

Abstract

We compare measurements from the Aeronomy of Ice in the Mesosphere (AIM) Cloud Imaging and Particle Size experiment (CIPS) to the NOAA-17 Solar Backscatter Ultraviolet instrument (SBUV/2) during the 2007 northern hemisphere Polar Mesospheric Cloud (PMC) season. Daily average Rayleigh scattering albedos determined from identical footprints from the CIPS nadir camera and SBUV/2 agree to better than ~5% throughout the season. Average PMC brightnesses derived from the two instruments agree to within ±10%. PMC occurrence frequencies are on average ~5% to nearly a factor of two higher in CIPS, depending on latitude. Agreement is best at high latitudes where

47 clouds are brighter and more frequent. The comparisons indicate that AIM CIPS data are
48 valid for scientific analyses. They also show that CIPS measurements can be linked to the
49 long time series of SBUV/2 data to investigate long-term variability in PMCs.
50
51 Keywords: Polar Mesospheric Cloud, PMC, SBUV, AIM, Validation, Noctilucent Cloud
52
53 1. Introduction
54 Polar Mesospheric Clouds (PMCs) are very thin ice clouds forming in the summer
55 mesopause region. It has been suggested that they are related to climate change in the
56 upper atmosphere (Thomas, 1996a and Thomas et al., 1991). As tracers of upper
57 atmosphere water vapor (H_2O) and temperature, PMCs can be used to understand the
58 dynamics of the upper mesosphere. Thomas et al. (1989) first suggested that increases in
59 mesospheric H_2O resulting from increased methane would lead to brighter PMCs.
60 Thomas (1996b) proposed that this could cause PMCs to shift to lower latitudes and
61 altitudes, and whereas DeLand et al. (2003) suggested that it might lead to an earlier first
62 appearance of PMCs during evening twilight. AIM is the first satellite mission
63 specifically dedicated to measuring PMCs. The mission is designed to elucidate the
64 connections between PMCs and mesospheric H_2O, temperature, and dynamics, with an
65 overall goal of understanding how PMCs form and why they vary (Russell et al., 2008).
66
67 The Cloud Imaging and Particle Size experiment (CIPS) is a panoramic imager with a
68 field of view of 120° (along track) by 80° (cross-track) or about 2000 x 1000 km; it is
69 described in more detail by Russell et al. (2008) and McClintock et al. (2008). CIPS has

an unprecedented spatial resolution of ~2km in the nadir. In order to derive PMC morphology and cloud particle size, CIPS measures scattered sunlight with a 15 nm passband centered at 265 nm. The observed signals include Rayleigh scattering by atmospheric gases as well as scattering by the PMCs themselves. The Rayleigh scattering signal must therefore be separated from the observed signal to infer PMCs. The method by which this is accomplished is described below. Radiation at 265 nm penetrates to an altitude of about 50 km; the atmospheric Rayleigh scattering signal is thus modulated by upper stratospheric and mesospheric ozone absorption in the Hartley-Huggins band as the radiation propagates along the incident and scattered light paths. Chandran et al. (2008) take advantage of the ozone modulation to derive information regarding gravity waves. Merkel et al. (2008) analyze the clouds detected by CIPS to derive information on planetary wave activity in the mesosphere. Rusch et al. (2008) describe features in the CIPS cloud data that are likely caused by various dynamical phenomena.

The primary goal of this paper is to show that the AIM CIPS data are of high quality, and valid for the types of scientific analyses described above. This is accomplished by comparing CIPS measurements to concurrent measurements from the NOAA-17 Solar Backscatter Ultraviolet (SBUV/2) instrument (e.g., Frederick et al., 1986; Heath et al., 1975). The SBUV instruments have a long history of PMC measurements, spanning several decades. Therefore, these comparisons also accomplish the goal of showing that the CIPS measurements can be linked to the long time series of SBUV data to investigate long-term variability in PMCs. Because of the coincident atmospheric information available from the Solar Occultation For Ice Experiment (SOFIE) (Russell et al., 2008)

93 and the Sounding of the Atmosphere using Broadband Emission Radiometry (SABER)
94 (Russell et al., 1999), we can ultimately address the question of the origin of long-term
95 variability, one of the scientific objectives of AIM.
96
97 The SBUV/2 instruments are nadir-pointed, and measure backscattered radiation at 12
98 different wavelengths ranging from 252-340 nm. Unlike CIPS, the SBUV/2 instruments
99 are not imagers; rather, the field of view consists of a single footprint of 11.3° × 11.3°, or
100 about 150 km × 150 km at the PMC altitude. The SBUV/2 instruments were originally
101 designed to measure ozone, but have been used extensively to measure PMCs (Thomas et
102 al., 1991; DeLand et al., 2003; 2006; 2007). For the comparisons shown here, the CIPS
103 data were analyzed in the same manner as the SBUV/2 data, as described in the next
104 section. We use level 1a CIPS data, version 3. We restrict the comparisons here to the
105 NOAA-17 SBUV/2 data, since the local times of measurements from this satellite more
106 closely match the CIPS local times than measurements from other SBUV/2 instruments.
107 The SBUV/2 data correspond to version 3. SBUV data have been validated extensively
108 with instruments measuring profile and column ozone as well as PMCs. The integrated
109 ozone columns measured by SBUV and the Stratospheric Aerosol and Gas Experiment
110 between October 1984 and June 1990 agree to within ±2.3% at all latitudes (McPeters et
111 al., 1994). Thomas et al. (1991) showed that SBUV correlates well with Solar
112 Mesosphere Explorer (SME) PMC data: the seasonal and latitudinal variations of PMCs
113 are similar, and correcting for different sensitivities of the instruments, the general
114 magnitude of the SBUV residuals is consistent with that expected from SME data.
115 DeLand et al. (2003) extended this comparison to SBUV/2 and found that NOAA-9

SBUV/2, Nimbus-7 SBUV and SME results for the 1985 and 1986 season were very similar in magnitude and temporal structure when different sensitivities and scattering angles were accounted for.

2. Cloud Detection Algorithm

Both the SBUV/2 and CIPS instruments measure radiance backscattered by the atmosphere and clouds. The albedo (unit of sr^{-1}) is obtained by dividing the radiance by the solar irradiance; an albedo of 1.0×10^{-6} sr^{-1} is defined here as 1 "Gary" (G). This section describes the method by which we separate the contributions to the albedo from "background" Rayleigh scattering and PMC scattering. As described by Bailey et al. (2008), one approach to separating Rayleigh scattering from cloud scattering takes advantage of the fact that CIPS is capable of measuring the scattering phase function. That is, CIPS takes multiple exposures of the same region of the atmosphere at different scattering angles. Since scattering by the relatively large particles in clouds corresponds to a different phase function than Rayleigh scattering, this technique can be utilized to separate the background Rayleigh scattering from the PMCs. This approach is not possible with the SBUV/2 instrument, since it does not measure the same region of space at multiple scattering angles. Thus the technique used for the CIPS/SBUV comparisons is based on a simplification of the method described by DeLand et al. (2003), which is applied to both the CIPS and SBUV/2 data.

In the SBUV/2 data, PMCs appear as spectrally dependent enhancements of the background (Rayleigh scattering) signal. Since the CIPS instrument does not have multi-

wavelength data, the standard SBUV/2 cloud detection algorithm, which takes advantage of the spectral dependence, cannot be applied directly to the CIPS data. Therefore, the standard algorithm was modified to a single-wavelength approach, and the modified algorithm was applied to both the SBUV/2 and CIPS data. Here we describe the standard SBUV/2 algorithm, then compare results from it to the modified algorithm.

In the standard SBUV/2 analysis, the background albedo is defined as a 4th order polynomial fit to the observed albedo as a function of solar zenith angle (SZA), including all measurements on a given day. The fit is calculated for data acquired at each of five UV wavelengths (DeLand et al., 2003). As an example, the top left plot of Figure 1 shows the SBUV/2 albedo as a function of SZA at 273 nm on 20 July 2007. Filled, blue circles depict clouds; open, black circles depict non-clouds (background); and the red line represents the polynomial fit to the background. For a nadir instrument like SBUV/2 the SZA can be converted to the solar scattering angle (SCA): SCA = 180° - SZA. Therefore, the background albedo decreases (increases) with increasing SZA (SCA) between 0 and 90° SZA (90 and 180° SCA), as expected for Rayleigh scattering. The difference between the albedo values and the background fit is defined as the albedo residual or, for clouds, the PMC brightness for each wavelength. The residuals for this example are shown in the bottom left plot of Figure 1. Again, filled and open circles depict cloud and non-cloud points.

In order to identify clouds in the SBUV/2 data, the standard algorithm applies several wavelength-dependent tests to the albedo residuals, as described by DeLand et al. (2003)

and updated by DeLand et al. (2007). The first test requires that the albedo residuals at the three shortest wavelengths are positive. The second test is based on the fact that for the small particle sizes expected of PMCs, the PMC scattering will be stronger at shorter wavelengths; this imposed the requirement that the slope of a linear regression fit to the five residuals be negative. Other tests require the 252-nm albedo residual to exceed the 273-nm albedo residual and the albedo to exceed a noise threshold. The last test requires the residual to exceed the smaller of either an absolute (7 G) or relative (1.05 times the average background) threshold. The last test will be referred to as the absolute/relative threshold test. All these tests are run five times iteratively, with successive iterations including only those points that were identified as "background". After five iterations, the points that have not passed the tests on any iteration are identified as background, and all others are identified as clouds. The left panels of Figure 1 show SBUV/2 cloud identifications for 20 July 2007 that were based on this multi-wavelength identification procedure.

For application to CIPS data, which measures at only one wavelength, the algorithm was modified to require only that the residuals for clouds be positive and pass the absolute/relative threshold test. In the following, the original cloud detection algorithm described by DeLand et al. (2003; 2007) will be referred to as the "all-λ" algorithm, whereas the modified algorithm will be referred to as the "one-λ" algorithm. To estimate the error introduced by removing the spectral information from the cloud identification algorithm, the one-λ algorithm was applied to SBUV/2 data and the results compared to those obtained using the all-λ algorithm. The SBUV/2 wavelength used was 273 nm,

185 which is the SBUV/2 channel that is closest to the center of the CIPS bandpass at 265 nm.
186 When the albedos of CIPS and SBUV/2 are normalized to account for the different
187 instrument bandpasses and spectral dependence of the solar irradiance, it fortuitously
188 turns out that the normalization is identically 1.0 for the 273-nm SBUV/2 channel.
189 Further, this channel has a signal to noise ratio that is ~4-5 times higher than the 252-nm
190 channel.
191
192 Figure 1 illustrates the comparisons between the all-λ and one-λ algorithms with a single
193 day of data on 20 July 2007. As noted above, the left panels display clouds identified
194 with the all-λ algorithm; the right panels display clouds identified with the one-λ
195 algorithm. The occurrence frequency, which is defined as the ratio of the number of cloud
196 observations to the number of measurements per day, was 19.1% with the all-λ algorithm
197 and 26.8% with the one-λ algorithm. The one-λ cloud detection algorithm results in a
198 higher occurrence frequency because fewer tests are required, making it less stringent.
199 The bottom panels of Figure 1 clearly differentiate between the clouds and background,
200 showing that there is no systematic pattern with respect to SZA. Most of the clouds
201 detected by the one-λ algorithm that are not detected by the all-λ algorithm have
202 brightnesses that are close to the background (non-cloud) level, but not all. In general,
203 however, the one-λ algorithm gives results that are close to the all-λ algorithm. This is
204 represented statistically in Figure 2, which shows the occurrence frequency vs. day of
205 year for the one-λ and all-λ algorithms, for all SBUV/2 data over the entire northern
206 hemisphere (NH) season in 2007. The one-λ algorithm reproduces the temporal variation
207 in cloud frequencies very well throughout the season, but with a high bias. The average

208 frequency over the whole season is 11% for the one-λ case and 8% for the all-λ case.
209 Note that results are similar if only the brightest clouds are included in the analysis. We
210 conclude from this analysis that the one-λ algorithm is suitable for comparing CIPS and
211 SBUV/2 data to evaluate the CIPS data, although frequencies might be overestimated for
212 both instruments.
213
214 To further ensure that the data sets are analyzed in a consistent manner, the CIPS
215 measurements were binned into a footprint that matches the SBUV/2 footprint of ~150
216 km × 150 km at cloud altitude. Thus a single SBUV/2 measurement corresponds to the
217 average of more than 5000 CIPS pixels. This results in an improvement in signal to noise
218 ratio from 5.2 in a single-pixel measurement of the background Earth albedo (Russell et
219 al., 2008) to more than 350 for the binned data. Figure 3 illustrates the viewing
220 geometries of CIPS and SBUV/2; all CIPS pixels within the SBUV/2 footprint indicated
221 in blue were binned together for the comparisons described below. Results are shown
222 below for the CIPS PY camera (see Figure 3), but they are essentially identical for the
223 MY camera.
224
225 3. Results and Discussion
226 An accurate retrieval of the Rayleigh background is fundamental for proper cloud
227 detections. Figure 4 compares the background polynomial fits to CIPS and SBUV/2 data
228 for 30 August 2007, a day when no clouds were detected. The top plot shows the albedo
229 vs. SZA, with CIPS in red and SBUV/2 in blue. The bottom plot shows the percent
230 difference between the two instruments in the overlapping SZA ranges. For this day the

231 CIPS background is on average about 2% lower than the SBUV/2 background,
232 representing one of the more favorable comparisons in the data set. Differences are
233 largest at low solar zenith angles, which is likely explained by the fact that the
234 measurement latitudes are significantly different at these SZA values. Figure 5 gives an
235 overview of the background differences vs. day of year in 2007. The differences here are
236 calculated as the average of the differences vs. solar zenith angle on each day (e.g., the
237 average of the bottom curves in Figure 4, averaged over the entire season). Squares
238 denote the mean background differences for days on which no clouds were detected.
239 CIPS is systematically lower than SBUV/2, but differences are smaller than 5%, with the
240 exception of one day in July.
241
242 There is an interesting time dependence in the background differences. At the beginning
243 and end of the time period, when few or no clouds are present, the agreement is better
244 than in the middle of the season. This could suggest that clouds lead to larger background
245 differences, but this suggestion is contradicted by the behavior of the differences in the
246 middle of the season. That is, temporal variations during the cloud season appear to
247 reflect some of the same variations seen in the cloud frequencies in Figure 2. Peaks in
248 frequency occur near 0 and 30 days since solstice; this corresponds approximately to
249 decreases, not increases, in the background differences shown in Figure 5. One
250 explanation for this apparent contradiction pertains to the relative brightness of the clouds
251 that are present. Correct calculation of the background requires identification of clouds
252 above the background variability, which is caused primarily by fluctuations in ozone
253 densities [e.g., DeLand et al., 2007] and measurement error. At the beginning and end of

254 the season, clouds are less frequent and on average relatively dim, so even incorrect
255 identification does not lead to significant errors in the background calculation. In the
256 middle of the season, however, incorrect identification of relatively dim clouds can lead
257 to significant errors in the background because the clouds are so much more numerous.
258 The larger or relatively brighter clouds are more easily distinguished from the
259 background variability, and thus are not expected to lead to significant errors. As shown
260 below (see Figure 9), near days 0 and 30 when the cloud frequencies increased, the
261 average cloud brightness also increased. Thus, we speculate that the background
262 calculations should improve near days 0 and 30 since the brighter clouds present at these
263 times are more easily identified, and therefore do not contaminate the background
264 calculation.
265
266 Figure 6 shows cloud detections for 22 June 2007 from both SBUV/2 (left) and CIPS
267 (right). The top (bottom) plots show albedo (albedo residual) vs. SZA, with clouds
268 denoted in filled blue (red) symbols for the SBUV/2 (CIPS) instruments. Both the albedo
269 and albedo residual values compare well with each other, with a minimum near 60-65°
270 SZA and relative maxima near 55° and 70° SZA. The CIPS occurrence frequency of
271 20.6% is higher than the 16.7% occurrence frequency of SBUV/2; this is discussed more
272 below. Interestingly, the background (non-cloud) residuals here are very similar in the
273 SBUV/2 and CIPS data. Since the binned CIPS data have such low noise (<0.5%), the
274 variability seen here is very likely real, and caused by ozone fluctuations.
275

Figure 7 shows a qualitative comparison of the latitude dependence of CIPS and SBUV/2 cloud frequencies throughout the season. Both instruments show an asymmetric pattern, with cloud frequencies reaching maximum latitudinal extent near the summer solstice just a few weeks after the first clouds were observed, before gradually diminishing in extent over the next 60 days. Both instruments also show a marked decrease in frequency about 10-20 days after solstice that extends across all latitudes. These kinds of patterns have also been noted in other satellite observations of PMCs (e.g., Bailey et al., 2005). Noteworthy is that, consistent with the single-day result in Figure 6, the CIPS frequencies are generally higher than the SBUV/2 frequencies throughout the season and at all latitudes, as quantified next.

Figures 8 and 9 compare the occurrence frequency and PMC brightness for three different latitude ranges (60-70°N, 70-80°N, and 80-83°N) for CIPS (red) and SBUV/2 (blue). The third latitude range extends only to 83°N because this is the highest latitude either instrument samples. Overall both the frequency and brightness of the two instruments compare very well to each other, but with some latitude dependence. The CIPS frequency is higher than the SBUV/2 frequency, as already noted, but the morphology is similar. Averaged over the season, the frequencies for CIPS (SBUV) are 8% (4%), 19% (15%), and 23% (22%) for the latitude bands from 60-70°N, 70-80°N, and 80-83°N, respectively. That frequencies compare better at higher latitudes might be due in part to the fact that measurement locations for the two instruments are closer together at the high latitudes. It is probably also related to the fact that cloud brightness increases with increasing latitude, as shown in Figure 9. Cloud detections are more robust for the

299 brighter clouds because they are easier to distinguish from the background (DeLand et al.,
300 2007). The average cloud brightnesses for CIPS (SBUV/2) are 6.7 G (7.4 G), 10.3 G
301 (10.0 G), and 12.2 G (11.2 G) for the respective latitude bands. Thus on average the
302 brightnesses derived from CIPS and SBUV/2 agree to within 10%. We speculate that the
303 higher CIPS frequencies at the lower latitudes arise because low-intensity clouds are
304 more likely to be detected as noise on the background in the SBUV data, but actual
305 clouds in the CIPS data. This is also consistent with the background comparisons shown
306 in Figure 5. If low-intensity clouds are identified incorrectly as background in the
307 SBUV/2 data, they will raise the background level, resulting in a background in CIPS that
308 is lower than in SBUV/2.
309
310 The results shown above include all of the available measurements from the two
311 instruments, regardless of location and local time. To examine the possibility that these
312 results were biased because of different measurement sampling, comparisons were
313 repeated using only those measurements from both instruments that were within 100 km
314 and 1 hour in local time. Although geophysical variations can take place on these scales,
315 this was considered a reasonable trade-off between minimizing differences in the
316 observed atmospheric region and obtaining significant statistics. Figure 10 shows the
317 SBUV/2 and CIPS nadir locations on 27 June 2007 (symbols do not correspond to actual
318 footprint size). The framed symbols depict the coincidences. All symbols are color coded
319 for their local time. The left plot shows the measurement locations for the whole latitude
320 range of the measurements for that day (40-90°), whereas the right plot is restricted 75 to
321 90° in order to better display the coincidences. Over the entire season there were 1372

322 coincidences between CIPS and , or about 16 coincidences per day (ranging from 9 to 23).
323 Most coincidences were between 78 and 82°N because local time changes rapidly as the
324 satellites cross the polar cap and go from the day side into the night side of the Earth.
325 Note that the number of coincidences is limited by the nadir-viewing constraint we have
326 placed on the current analysis; many more coincidences will be available for future
327 comparisons using all CIPS viewing angles.
328
329 Figure 11 shows the results of the coincidence comparisons. The full cloud-detection
330 analysis was not repeated because the lack of data compromises the background
331 simulation. Rather, for Figure 11 the daily average quantities were simply re-calculated
332 using only the coincident data points, but utilizing the background albedo derived with
333 the full data set. To the extent that different measurement sampling affects the
334 background determination, these results are similar to the non-coincident results shown
335 above; they should, however, be less affected by PMC variability. Figure 11 shows the
336 comparisons for daily average albedo (cloud + background), frequency, and daily average
337 albedo residual (albedo minus background) for all coincident measurements. As expected
338 from the comparisons discussed above, all three panels show excellent agreement. The
339 average albedo over the season was 149 G (154 G) for CIPS (SBUV/2), a difference of
340 only 3%. The average daily cloud frequency over the season was 24% (27%), and the
341 average cloud brightness over the season was 13% (12%) for CIPS (SBUV). These
342 results are similar to the results of the non-coincidence analysis, suggesting that sampling
343 issues are not a significant factor in the comparisons.
344

4. Conclusions

We have described comparisons between AIM CIPS and SBUV/2 Rayleigh scattering and PMC scattering measurements. A single cloud detection algorithm was applied to data from both instruments, and the high spatial resolution CIPS data were binned to match the SBUV/2 footprint. The CIPS data were thus restricted to the nadir, while SBUV/2 data were restricted to the 273-nm channel. The cloud detection algorithm was based on the standard SBUV/2 cloud detection algorithm, but ignored all spectral information.

The comparisons show that CIPS and SBUV/2 measurements are in excellent agreement. The daily average Rayleigh scattering backgrounds determined from the two instruments agree to better than ~5% throughout the season. Average CIPS PMC brightnesses are within 10% of the SBUV values. CIPS daily PMC occurrence frequencies are generally higher than those from SBUV/2, with differences decreasing at high latitudes where the clouds are brighter and more frequent. From 60-70°N the average frequencies differed by a factor of two, but this decreased to less than 5% from 80-83°N. We tentatively attribute the frequency differences to the fact that binning the CIPS data into the SBUV footprint significantly improves the signal-to-noise, making it more likely that dim clouds are properly identified as such in the CIPS data. We note, however, that the single-wavelength algorithm applied here does not take advantage of the full capabilities of the SBUV/2 data, since it ignores spectral information.

367 We conclude from the above comparisons that the CIPS nadir data are valid for scientific
368 analysis. It should be noted that only a tiny fraction of the available CIPS data has
369 actually been used. Nadir data within the SBUV/2 footprints from the PY camera
370 represent less than 0.001% of the CIPS data. In the analysis presented above, the high
371 spatial resolution of the CIPS data as well as the scattering angle dependence has been
372 lost. Extended algorithms are necessary to take advantage of these unique CIPS features,
373 such as described by Bailey et al. (2008). Data produced with this type of extended
374 algorithm was used in the analyses of Chandran et al. (2008), Rusch et al. (2008) and
375 Merkel et al. (2008). Although the current paper does not provide direct validation of the
376 data used in those papers, the above results do indicate that the cameras are performing as
377 expected. Further, the results in the nadir pixels analyzed here are consistent with the
378 broader results described in these other papers. An example is shown here in Figure 12.
379 This figure portrays the average NH PMC occurrence frequency as a function of day and
380 longitude during the 2007 season, for latitudes from 75-85°N. SBUV/2 results are shown
381 in the left panel; CIPS results (right) include only the data binned into the SBUV/2
382 footprint. Not only do the results agree with each other, as expected from the
383 comparisons shown above, but they also agree with the more comprehensive analysis
384 described by Merkel et al. (2008). That paper uses all of the CIPS data to explore the
385 occurrence of planetary wave activity in the CIPS data, which is seen clearly in both the
386 nadir CIPS and SBUV/2 data here. The comparisons shown here thus serve not only to
387 validate the nadir CIPS data, but also to lend credibility to the off-nadir measurements as
388 well. Finally, that CIPS data compare so well to SBUV/2 data supports the goal of

389 linking the long time series of SBUV/2 data to the CIPS data in order to investigate long-
390 term variability in PMCs.
391
392 Acknowledgements: Funding for CIPS data evaluation, and for the AIM mission, was
393 provided by the NASA Small Explorer program. The SBUV/2 data were obtained from
394 NOAA/NESDIS with support from the NOAA Climate and Global Change Atmospheric
395 Chemistry Element. Some of this work was supported by grant NNX06AC96G from
396 NASA's Office of Space Science.
397
398 References
399 Bailey, S.M., A.W. Merkel, G.E. Thomas, and J.N. Carstens, 2005. Observations of polar
400 mesospheric clouds by the Student Nitric Oxide Explorer, J. Geophys. Res. 110, D13203,
401 doi:10.1029/2004JD005422, 2005.
402 Bailey, S.M., et al., 2008. Phase Functions of Polar Mesospheric Cloud Ice as Observed
403 by the CIPS Instrument on the AIM Satellite. JASTP, this issue.
404 Chandran, A., et al., 2008. Gravity wave observation from the Cloud Imaging and
405 Particle Size (CIPS) Experiment on the AIM Spacecraft. JASTP, this issue.
406 DeLand, M.T., E.P. Shettle, G.E. Thomas, and J.J. Olivero, 2003. Solar backscattered
407 ultraviolet (SBUV) observations of polar mesospheric clouds (PMCs) over two solar
408 cycles. J. Geophys. Res., 108 (D8), 8445, doi:10.1029/2002JD002398.
409 DeLand, M.T., E.P. Shettle, G.E. Thomas, and J.J. Olivero, 2006. A quarter-century of
410 satellite polar mesospheric cloud observations. JASTP 68, 9-29.

411 DeLand M. T., E. P. Shettle, G. E. Thomas, J. J. Olivero, 2007. Latitude-dependent long-
412 term variations in polar mesospheric clouds from SBUV version 3 PMC data. J. Geophys.
413 Res., 112, D10315, doi:10.1029/2006JD007857.
414 Frederick, J.E, R.P. Cebula, & D.F. Heath, 1986. Instrument characterization for the
415 detection of long-term changes in stratospheric ozone: An analysis of the SBUV/2
416 radiometer. J. Atmos. Oceanic Technol., 3, 472-480.
417 Heath, D.F., et al., 1975. The solar backscatter ultraviolet and total ozone mapping
418 spectrometer (SBUV/TOMS) for Nimbus G. Optical Engineering, 14, 323-331.
419 McClintock, W., et al., 2008. The Cloud Imaging and Particle Size (CIPS) Experiment on
420 the Aeronomy of Ice in the Mesosphere (AIM) Spacecraft. JASTP, this issue.
421 McPeters, R.D., T. Miles, L.E. Flynn, C.G. Wellemeyer, and J.M. Zawodny, 1994.
422 Comparison of SBUV and SAGE II ozone profiles: Implications for ozone trends. J.
423 Geophys. Res. 99, 20513.
424 Merkel, A.W., et al., 2008. Planetary wave activity in Polar Mesospheric Clouds as
425 observed from the Cloud Imaging and Particle Size instrument. JASTP, this issue.
426 Rusch, D.W., et al., 2008. The Cloud Imaging and Particle Size Experiment on the
427 Aeronomy of Ice in the Mesosphere Mission: Cloud Morphology for the Northern 2007
428 season, JASTP. this issue.
429 Russell, J.M., M.G. Mlynczak, L.L. Gordley, Larry , J. J. Tansock, and R. Esplin, 1999.
430 An overview of the SABER experiment and preliminary calibration results, Proc. SPIE
431 Vol. 3756, 277-288.
432 Russell, J.M., III, et al., 2008. The Aeronomy of Ice in the Mesosphere (AIM) Mission:
433 Overview and Early Science Results. JASTP, this issue.

434 Thomas, G.E., Olivero, J.J., 1989. Climatology of polar mesospheric clouds, 2. Further
435 analysis of Solar Mesospheric Explorer data. Journal of Geophysical Research 94,
436 14,673–14,702.
437 Thomas, G.E. et al., 1991. Satellite observations of polar mesospheric clouds by the solar
438 backscattered ultraviolet radiometer: evidence of a solar cycle dependence. JGR 96, 927–
439 939.
440 Thomas, G.E., 1996a. Is the polar mesosphere the miner's canary of global change?. Adv.
441 Space Res. 18, 149-158.
442 Thomas, G.E., 1996b. Global change in the mesosphere-lower thermosphere region: has
443 it already arrived?. Journal of Atmospheric and Solar-Terrestrial Physics 58, 1629-1656.

Figure captions

Figure 1. Comparison of the albedo (top) and albedo residual (bottom) derived from the standard SBUV/2 cloud detection algorithm ("all-λ", left) and the modified, single-wavelength algorithm ("one-λ", right) applied to NOAA-17 SBUV/2 data from 20 July 2007. The one-λ algorithm uses the SBUV/2 273-nm channel. Albedo units on all plots are 10^{-6} sr^{-1}. Black, open circles denote non-cloud points; blue, filled circles denote cloud detections. Labels just above the horizontal axis in the top panels denote measurement latitudes. The red line in the top panels indicates the fourth order polynomial fit to the background.

Figure 2. Daily occurrence frequencies (number of clouds divided by the total number of measurements on any given day, in %) from NOAA-17 SBUV/2 data calculated using the all-λ (red) and 273-nm one-λ (blue) algorithms. Measurement latitudes are restricted to 50-90°N.

Figure 3. Viewing geometry for the CIPS cameras, with the SBUV/2 field of view (blue) superimposed.

Figure 4. Fourth order polynomial fits to the background albedo (top) for CIPS (red) and NOAA-17 SBUV/2 (blue) at 273 nm and the difference between the fits (bottom) for overlapping SZA ranges on 30 August 2007. Labels above (below) the bottom (top) horizontal axes give measurement latitudes for CIPS (SBUV).

Figure 5. Average difference between the polynomial fits to the background for CIPS and SBUV/2 at 273 nm vs. day of year for the NH in 2007. "Error" bars represent one-sigma standard deviation of the mean difference on each day.

Figure 6. Left: Similar to the right panels in Figure 1, but for NOAA-17 SBUV/2 data at 273 nm on 22 June 2007; blue symbols denote PMCs. Right: Same as left, but for CIPS data on 22 June 2007; red symbols denote PMCs. Albedo units are 10^{-6} sr^{-1}.

Figure 7. Daily PMC cloud occurrence frequency from NOAA-17 SBUV/2 data at 273 nm (top) and CIPS (bottom) in the NH in 2007. Occurrence frequencies (%) are calculated as the number of measurements identified as clouds relative to the total number of measurements in 2-degree latitude bins.

Figure 8. CIPS (red) and SBUV/2 (blue) PMC occurrence frequency vs. day of year for three different latitude ranges. Here the occurrence frequencies (in %) are calculated as the number of measurements identified as clouds relative to the total number of measurements in the latitude bins specified at the top of each panel.

Figure 9. Same as Figure 8, but for daily average albedo residuals pertaining to cloud detections in the specified latitude bins (observed albedo minus the polynomial fit to the background, so this represents the cloud brightness). The albedo residuals have units of 10^{-6} sr^{-1}. "Error" bars represent one-sigma standard deviation of the mean PMC albedo residual on each day.

Figure 10. Coincidences (framed symbols) overlaid on all measurements from CIPS (circles) and NOAA-17 SBUV/2 (stars) on 27 June 2007, for all latitudes (left) and only high latitudes (right). Symbols are color coded by their local time.

Figure 11. Daily average albedo (left), daily occurrence frequency (middle), and daily average PMC brightness (right, 10^{-6} sr^{-1}), for the NH 2007 season from CIPS (red) and NOAA-17 SBUV/2 at 273 nm (blue). Albedos are calculated as the average of the albedos at coincident measurement locations on each day. Albedo residuals are calculated similarly; the background subtracted from the albedo to yield the residual was determined from the full set of measurements, not just coincidences. Occurrence frequencies (%) refer to the number of coincident measurements identified as clouds relative to the total number of coincident measurements on each day.

Figure 12. Daily occurrence frequency from 75-85°N plotted vs. longitude for SBUV/2 at 273 nm (left) and CIPS (right) in the NH in 2007. Frequencies represent a running average over 20° in longitude. White, dashed lines are drawn only for guidance; they indicate the tilt that would be expected for a 5-day wave. See Merkel et al. (2008) for discussion of wave activity inferred from CIPS data.

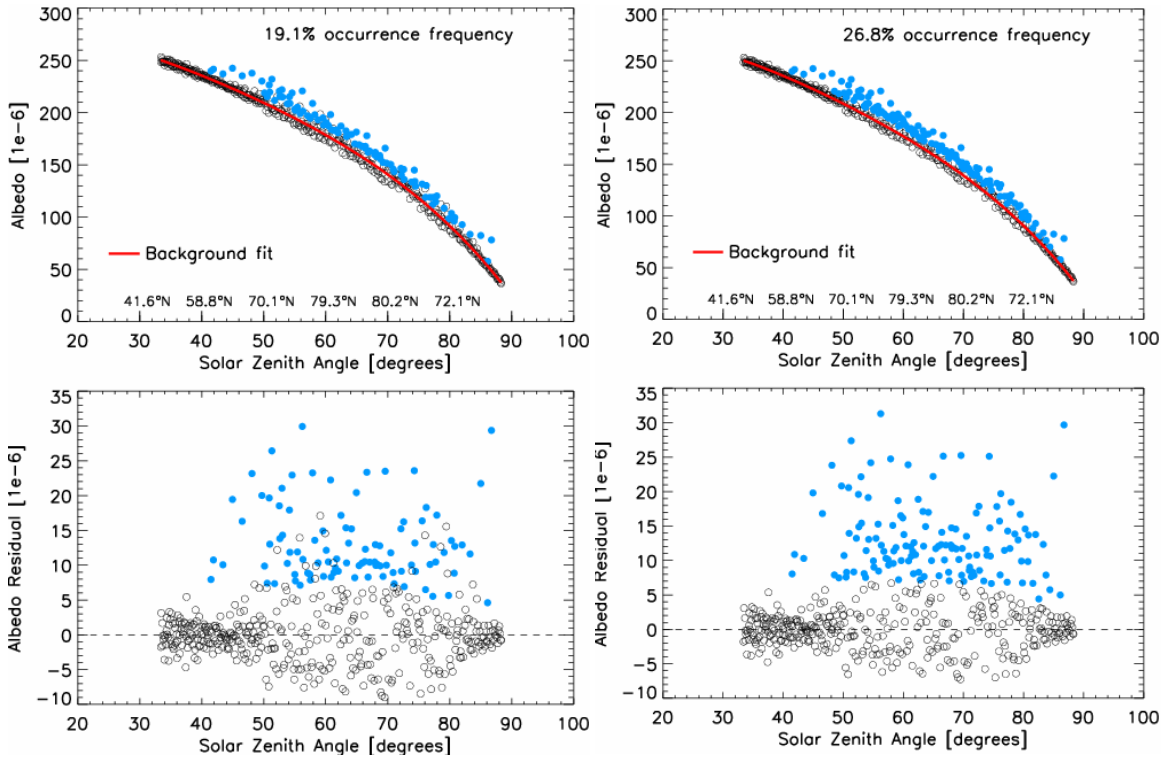

Figure 1. Comparison of the albedo (top) and albedo residual (bottom) derived from the standard SBUV/2 cloud detection algorithm ("all-λ", left) and the modified, single-wavelength algorithm ("one-λ", right) applied to NOAA-17 SBUV/2 data from 20 July 2007. The one-λ algorithm uses the SBUV/2 273-nm channel. Albedo units on all plots are 10^{-6} sr^{-1}. Black, open circles denote non-cloud points; blue, filled circles denote cloud detections. Labels just above the horizontal axis in the top panels denote measurement latitudes. The red line in the top panels indicates the fourth order polynomial fit to the background.

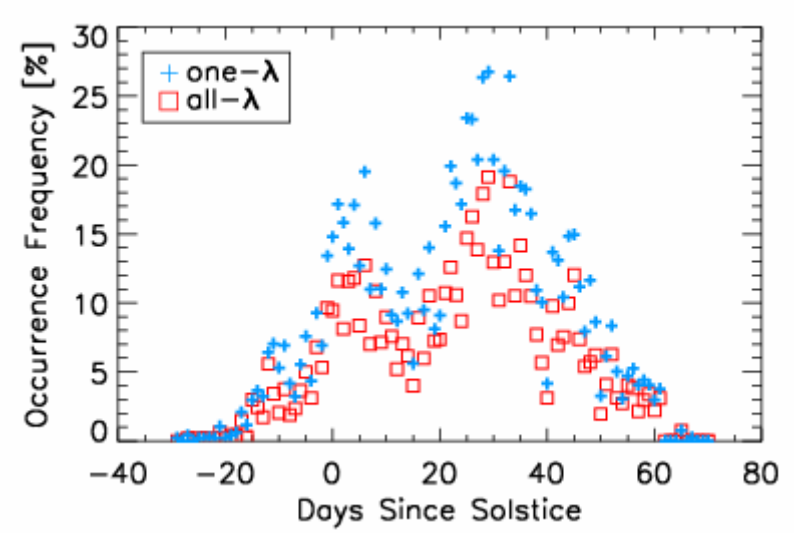

Figure 2. Daily occurrence frequencies (number of clouds divided by the total number of measurements on any given day, in %) from NOAA-17 SBUV/2 data calculated using the all-λ (red) and 273-nm one-λ (blue) algorithms. Measurement latitudes are restricted to 50-90°N.

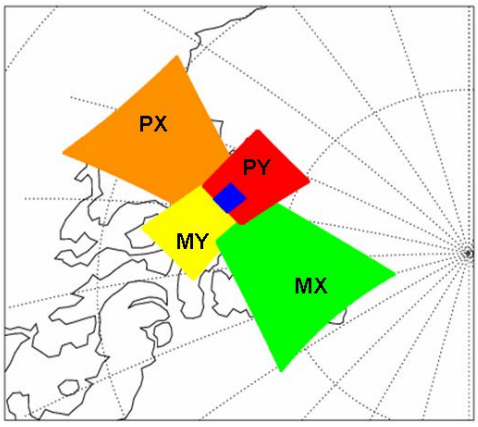

Figure 3. Viewing geometry for the CIPS cameras, with the SBUV/2 field of view (blue) superimposed.

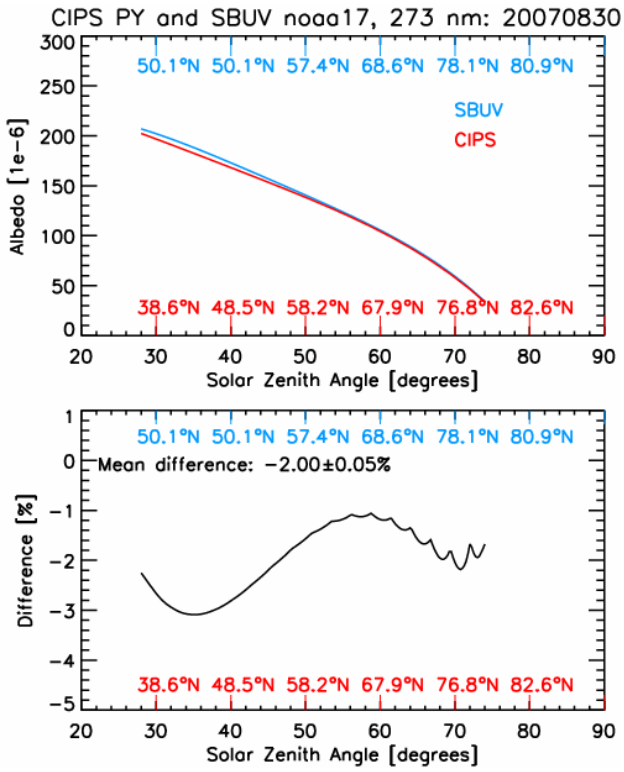

Figure 4. Fourth order polynomial fits to the background albedo (top) for CIPS (red) and NOAA-17 SBUV/2 (blue) at 273 nm and the difference between the fits (bottom) for overlapping SZA ranges on 30 August 2007. Labels above (below) the bottom (top) horizontal axes give measurement latitudes for CIPS (SBUV).

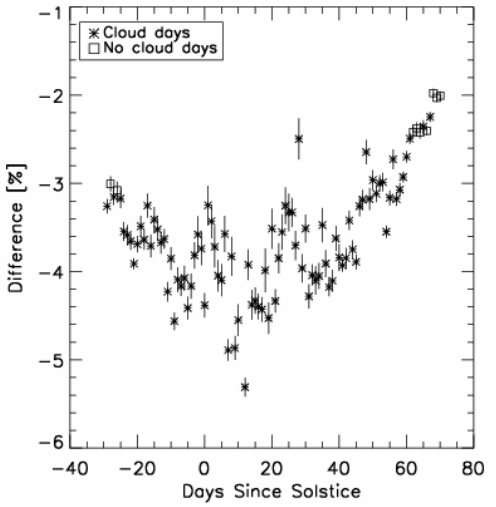

Figure 5. Average difference between the polynomial fits to the background for CIPS and SBUV/2 at 273 nm versus day of year for the NH in 2007. "Error" bars represent one-sigma standard deviation of the mean difference on each day.

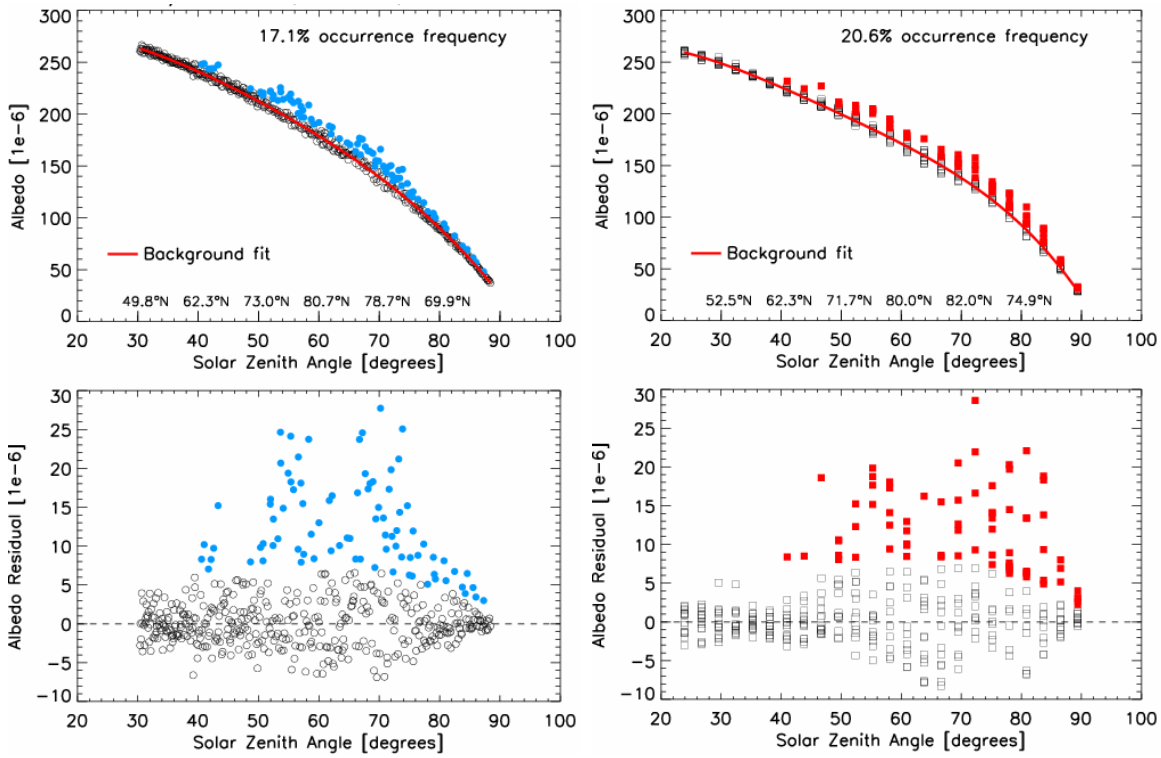

Figure 6. Left: Similar to the right panels in Figure 1, but for NOAA-17 SBUV/2 data at 273 nm on 22 June 2007; blue symbols denote PMCs. Right: Same as left, but for CIPS data on 22 June 2007; red symbols denote PMCs. Albedo units are 10^{-6} sr^{-1}.

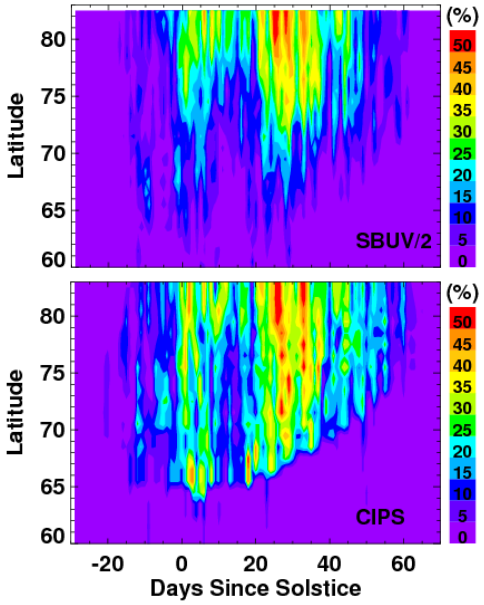

Figure 7. Daily PMC cloud occurrence frequency from NOAA-17 SBUV/2 data at 273 nm (top) and CIPS (bottom) in the NH in 2007. Occurrence frequencies (%) are calculated as the number of measurements identified as clouds relative to the total number of measurements in 2-degree latitude bins.

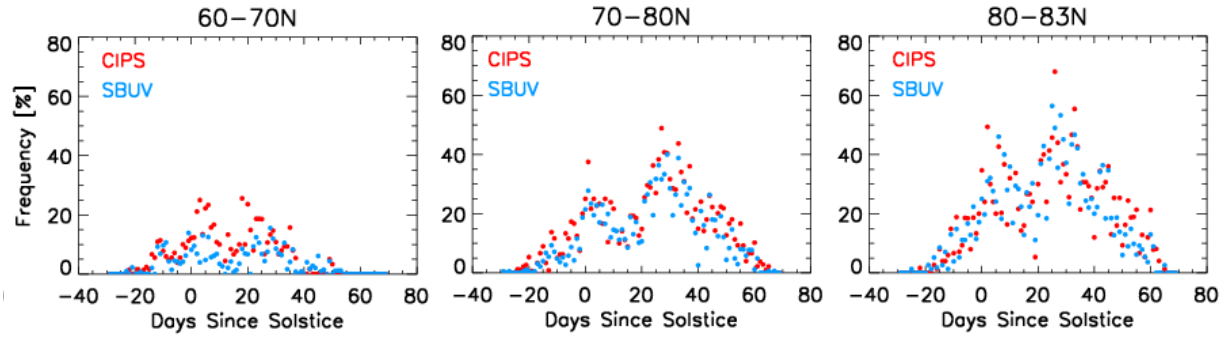

Figure 8. CIPS (red) and SBUV/2 (blue) PMC occurrence frequency versus day of year for three different latitude ranges. Here the occurrence frequencies (in %) are calculated as the number of measurements identified as clouds relative to the total number of measurements in the latitude bins specified at the top of each panel.

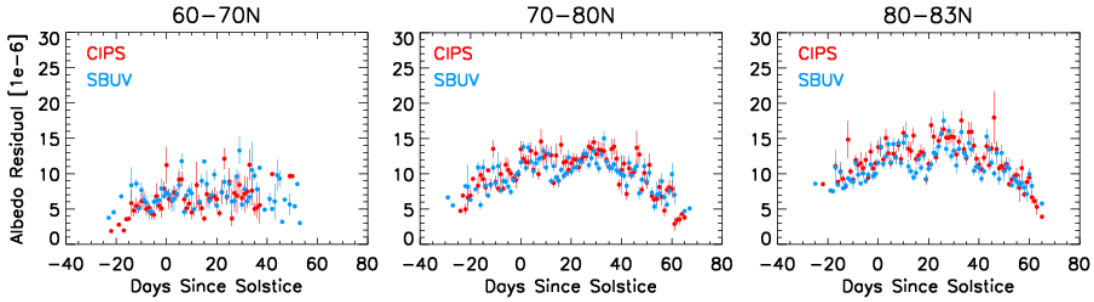

Figure 9. Same as Figure 8, but for daily average albedo residuals pertaining to cloud detections in the specified latitude bins (observed albedo minus the polynomial fit to the background, so this represents the cloud brightness). The albedo residuals have units of 10^{-6} sr^{-1}. "Error" bars represent one-sigma standard deviation of the mean PMC albedo residual on each day.

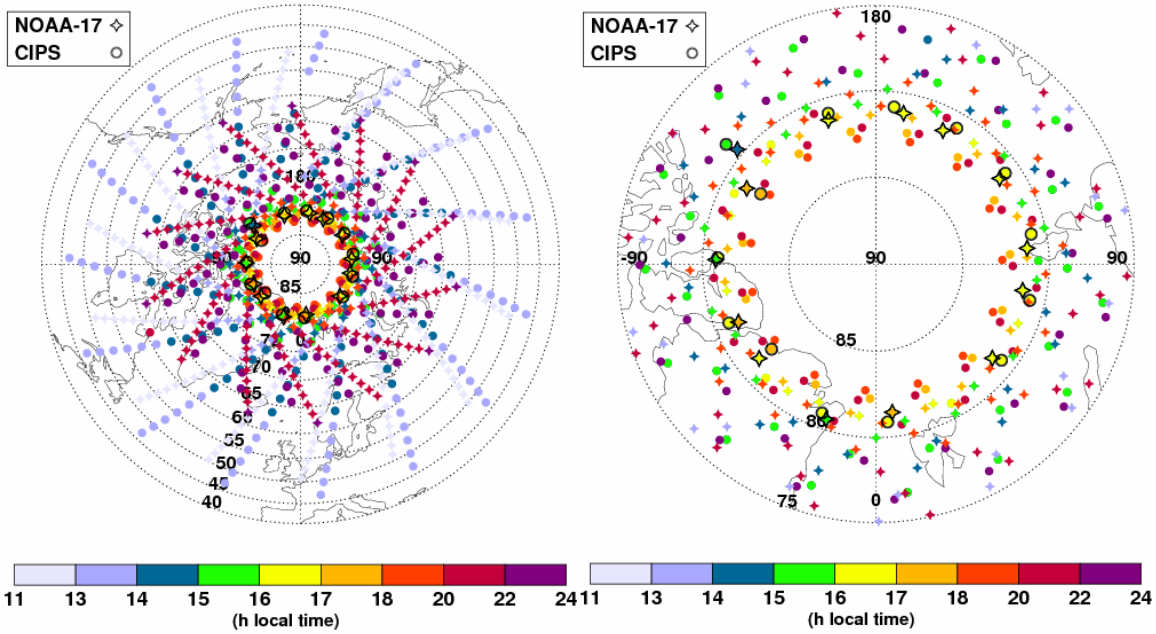

Figure 10. Coincidences (framed symbols) overlaid on all measurements from CIPS (circles) and NOAA-17 SBUV/2 (stars) on 27 June 2007, for all latitudes (left) and only high latitudes (right). Symbols are color coded by their local time.

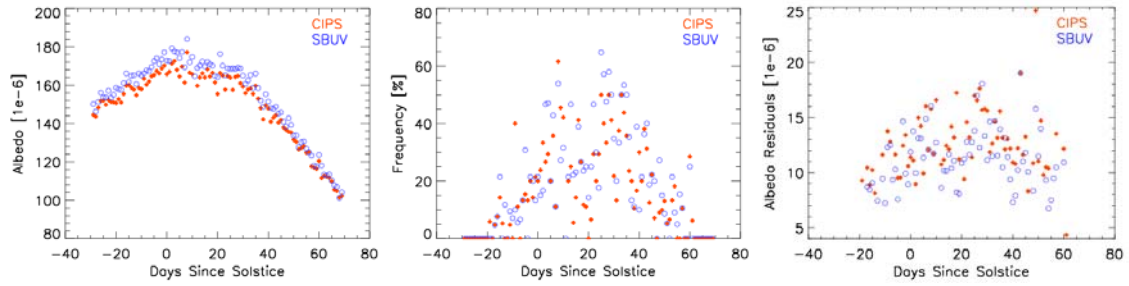

Figure 11. Daily average albedo (left), daily occurrence frequency (middle), and daily average PMC brightness (right, 10^{-6} sr^{-1}), for the NH 2007 season from CIPS (red) and NOAA-17 SBUV/2 at 273 nm (blue). Albedos are calculated as the average of the albedos at coincident measurement locations on each day. Albedo residuals are calculated similarly; the background subtracted from the albedo to yield the residual was determined from the full set of measurements, not just coincidences. Occurrence frequencies (%) refer to the number of coincident measurements identified as clouds relative to the total number of coincident measurements on each day.

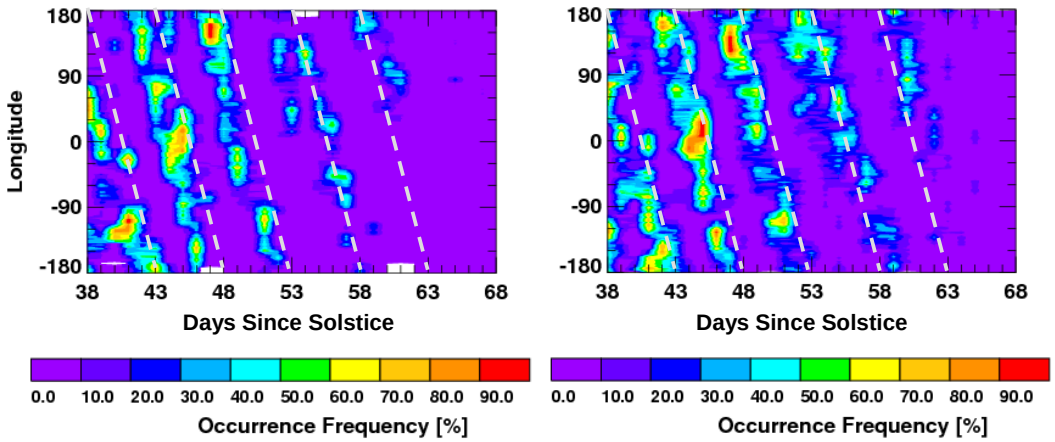

Figure 12. Daily occurrence frequency from 75-85°N plotted vs. longitude for SBUV/2 at 273 nm (left) and CIPS (right) in the NH in 2007. Frequencies represent a running average over 20° in longitude. White, dashed lines are drawn only for guidance; they indicate the tilt that would be expected for a 5-day wave. See Merkel et al. (2008) for discussion of wave activity inferred from CIPS data.